Nuclear versus electronic ring currents in oriented torsional molecules induced by magnetic fields. II. Electronic currents of toluene

Maria Dimitrova [1,*] Dongming Jia [2,†] Jörn Manz [3,4,5,‡] and Dage Sundholm [1,§]

[1]*Department of Chemistry, Faculty of Science, University of Helsinki, P.O. Box 55, A.I. Virtasen aukio 1, 00014 Helsinki, Finland*

[2]*MOE Key Laboratory for Nonequilibrium Synthesis and Modulation of Condensed Matter, School of Physics, Xi'an Jiaotong University, Xi'an 710049, China*

[3]*Institut für Chemie und Biochemie, Freie Universität Berlin, Takustraße 3, 14195 Berlin, Germany*

[4]*State Key Laboratory of Quantum Optics and Quantum Optics Devices, Institute of Laser Spectroscopy, Shanxi University, 92 Wucheng Road, Taiyuan 030006, China*

[5]*Collaborative Innovation Center of Extreme Optics, Shanxi University, 92 Wucheng Road, Taiyuan 030006, China*

(Received 8 February 2022; accepted 23 August 2022; published 3 October 2022; corrected 23 November 2022)

The theory of nuclear ring currents of torsional molecules induced by an external magnetic field along the torsion axis was developed in the preceding paper [D. Jia *et al.*, preceding paper, Phys. Rev. A **106**, 042801 (2022)]. Here we study the magnetically induced electronic current density (MIC) for toluene in the presence of an external magnetic field that is aligned with the torsion axis of the methyl group. Properties of the MIC are studied in detail at the density-functional theory (DFT) level using our gauge-including magnetically induced current method, the derivation of which is briefly outlined. The strength of the MIC is determined by numerical integration and compared to the estimated strength of the magnetically induced nuclear ring current reported in the preceding paper. Spatial contributions to the diatropic and paratropic MICs are discussed in detail, where the diatropic MIC flows in the classical direction and the paratropic MIC flows in the opposite direction. The MIC in the vicinity of the methyl group is mainly diatropic, whereas the phenyl group ring is dominated by a paratropic MIC of -14.90 nA T^{-1} localized to the carbon atoms. The strength of the MIC near the methyl group is 10.41 nA T^{-1}, which is of about the same size as the strength of the ring current of benzene when the magnetic field is perpendicular to the molecular ring. The strength of the magnetically induced nuclear ring current of the whole toluene molecule is 19.9 pA T^{-1}, which is two orders of magnitude smaller than the electronic one of -1.93 nA T^{-1} calculated for the eclipsed structure at the employed DFT level. This value is in perfect agreement with the current strength of -1.93 nA T^{-1} calculated at the coupled-cluster singles and doubles level with a perturbative treatment of the triple excitations. The current strength calculated at the second-order Møller-Plesset perturbation level is 1.20 nA T^{-1}, which is of the same size with opposite sign.

DOI: 10.1103/PhysRevA.106.042802

I. INTRODUCTION

The theory of nuclear ring currents in oriented torsional molecules induced by external magnetic fields was developed in the preceding paper [1]. The methods were demonstrated by performing calculations on toluene with the principal axis as the torsion axis, which coincides nearly perfectly with the C—C bond between the methyl group and the phenyl group. Since the torsional barrier of 0.0583 kJ/mol is very low [2], the methyl group rotates nearly freely. The barrier is even lower when vibrational coupling is taken into account [3]. Thus, the quantum-mechanical probability of observing the eclipsed or the staggered conformation is almost the same [3].

An external magnetic field along the torsional axis induces a rotation of the methyl group leading to a nuclear current density as described in the preceding paper [1,4]. The magnetic field induces an electronic current density around the methyl group. The aim of this work is to study the magnetically induced electronic current (MIC) density of toluene, when the magnetic field is oriented along the C—C bond to the methyl group. The MIC is calculated using the gauge-including magnetically induced current (GIMIC) method [5–9], which has previously been used in studies of the MIC of aromatic and antiaromatic molecules as well as in calculations of the current-density flux in porphyrinoids and nanostructures [7–13].

In the next section we present the electronic structure methods employed and describe how the molecular structure is optimized. The GIMIC method for calculating MICs is derived in Sec. III, where we also present the methodology used for analyzing the calculated MIC. The results of the MIC calculations are reported in Sec. IV. In Sec. V we discuss and summarize the results obtained.

II. MOLECULAR STRUCTURES AND COMPUTATIONAL LEVELS

The molecular structure of toluene was optimized at the density-functional theory (DFT) level with the B3LYP functional [14,15] using the def2-TZVP and the def2-QZVP

*maria.dimitrova@helsinki.fi
†dongmingjia123@gmail.com
‡jmanz@chemie.fu-berlin.de
§Corresponding author: sundholm@chem.helsinki.fi

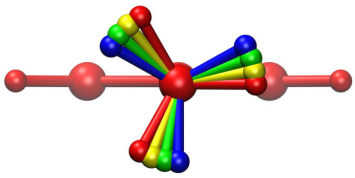

FIG. 1. The eclipsed conformer of toluene with the torsion angle $\varphi = 0^\circ$ is shown in red. The conformer with $\varphi = 10^\circ$ is yellow and $\varphi = 20^\circ$ is green. The staggered conformer with $\varphi = 30^\circ$ is shown in blue. The z coordinate points towards the reader.

basis sets [16]. The semiempirical D3-BJ correction was used to take dispersion interactions into account [17]. The calculations were performed with TURBOMOLE 7.4 [18–20]. The m5 integration grid was employed in the DFT calculations [21]. The gradient norm for the geometry optimization was 10^{-6} a.u., the energy convergence threshold for the single-point energy was 10^{-6} a.u., and the electron density convergence threshold was set to 10^{-7} a.u. The molecular structure of the staggered conformer with a torsion angle of 30° was optimized by enforcing the C_s symmetry point group. The DEFINE module of TURBOMOLE was used for the rotation of the methyl group in steps of 10° and the rest of the coordinates were subsequently optimized while keeping the dihedral angle frozen. The structures obtained are shown in Fig. 1. The rotational barriers were calculated at the B3LYP def2-TZVP and B3LYP def2-QZVP levels of theory as well as at the spin-component-scaled second-order Møller-Plesset perturbation (SCS-MP2) level using the def2-TZVPP basis set [16,22,23].

The def2-TZVP and def2-TZVPP basis sets of carbon consist of $5s3p2d1f$ basis functions. The def2-TZVP and the def2-TZVPP basis sets of hydrogen has $3s1p$ and $3s2p1d$ basis functions, respectively [16]. The def2-QZVP basis set is the largest basis set consisting of $4s3p2d1f$ basis functions for hydrogen and $7s4p3d2f1g$ for carbon [16], implying that the calculations with the def2-QZVP basis set is near the basis set limit at the DFT level.

The optimized molecular structure of toluene was used in the calculations of the nuclear magnetic resonance (NMR) shielding tensor at the B3LYP level with the def2-TZVP and def2-QZVP basis sets [16,24–26]. Nuclear magnetic resonance shielding tensors were also calculated at the MP2 level using the def2-TZVPP basis set [16,25,26] as well as the coupled-cluster single and double levels with a perturbational treatment of the triple excitations [CCSD(T)] [27] using Jensen's triple-ζ quality basis sets (pcseg-2) [28] with the CFOUR program [29–31]. The NMR shielding calculations provide the magnetically perturbed and the unperturbed density matrices which are used as input in the calculations of the magnetically induced current densities.

Rotational barrier

The energy difference between the eclipsed ($\varphi = 0^\circ$) and staggered ($\varphi = 30^\circ$) structures calculated at the B3LYP def2-QZVP level of theory for the optimized structures is 0.058 kJ/mol (4.83 cm^{-1}), which is in excellent agreement with the experimental value of 4.84 cm^{-1} [2]. The staggered conformer is lower in energy. When vibrational coupling is considered, the eclipsed structure is experimentally 1.57 cm^{-1} below the staggered one [3]. However, the small energy difference between the staggered and eclipsed structures implies that the methyl group is almost a free rotor, which is desirable when studying magnetically induced nuclear ring currents [1]. The energy difference between the staggered and eclipsed conformers of toluene calculated at different levels of theory in Table I shows that the barrier obtained at the B3LYP def2-QZVP level happens to agree with the experimental value, whereas the rotational barrier calculated at the *ab initio* levels is about a factor of 2 larger than the experimental one.

III. MAGNETICALLY INDUCED CURRENT-DENSITY METHODS

A. The GIMIC method

The GIMIC method has been employed to calculate current-density pathways and their strength in toluene [5,8]. The GIMIC program [32] is an open-source code interfaced with various program packages for molecular electronic structure calculations. It takes the magnetically perturbed and the unperturbed density matrices obtained in calculations of the nuclear magnetic shielding tensors as input data. The molecular structure given as the Cartesian coordinates of the atomic positions as well as basis-set information are also needed as input. The GIMIC method has been employed in studies of the MIC in molecules as well as to estimate the degree of molecular aromaticity [7–13]. Magnetically induced electronic currents can be investigated visually using streamline representations and quantitatively by integrating the strength of the current-density flux passing through the plane.

The MIC $\boldsymbol{j}_e^{\mathbf{B}}(\boldsymbol{r})$ is a vector quantity that can be expanded in a Taylor series with respect to the external magnetic field. For closed-shell molecules, the first term in Eq. (1) vanishes. The second term containing the current-density susceptibility $\mathcal{J}_e^{B_\beta}(\boldsymbol{r})$ is linear with respect to the strength of the external magnetic field, whereas higher-order terms can be omitted, because the interaction of magnetic fields that can be created in laboratories are in most cases weak compared to the electrostatic forces

$$\boldsymbol{j}_e^{\mathbf{B}}(\boldsymbol{r}) = \boldsymbol{j}_{e,0}(\boldsymbol{r}) + \sum_{\beta\in\{x,y,z\}} \left.\frac{\partial \boldsymbol{j}_e^{\mathbf{B}}(\boldsymbol{r})}{\partial B_\beta}\right|_{B_\beta=0} B_\beta + O\big(B_\beta^2\big). \quad (1)$$

The notation indicating that we consider *electronic* current densities is omitted in the following. The tensor elements of the first-order current-density susceptibility tensor are given by

$$\mathcal{J}_\alpha^{B_\beta}(\boldsymbol{r}) = \frac{\partial j_{e,\alpha}^{\mathbf{B}}(\boldsymbol{r})}{\partial B_\beta}, \quad (2)$$

where $\alpha, \beta \in \{x, y, z\}$. The current density, which is a vector function, is obtained by contracting the current-density susceptibility tensor $\mathcal{J}(\boldsymbol{r})$ with the components of the external magnetic field. The GIMIC expression for calculating $\mathcal{J}(\boldsymbol{r})$ was derived by combining the Biot-Savart expression for calculating the nuclear magnetic shielding tensor [33–36] with the corresponding analytic-gradient expression [37–39] as described in Refs. [5,6,8,9]. The Biot-Savart expression for the magnetic interaction energy between the nuclear magnetic moment $\mathbf{m}_K$ and the MIC consists of the integral of the vector

TABLE I. Energy difference (in kJ/mol) between the staggered and eclipsed conformers of toluene calculated at different levels of theory. The minimum of the potential energy surface is for the torsion angle $\varphi = 30^\circ$, while the maximum is at $\varphi = 0^\circ$. The molecular structures were optimized at the B3LYP def2-TZVP level.

Method Basis set / Tortion angle	B3LYP def2-TZVP	B3LYP def2-QZVP	SCS-MP2 def2-TZVPP	CCSD pcseg-2	CCSD(T) pcseg-2
0°	0.038	0.058	0.111	0.098	0.131
10°	0.030	0.045	0.083		
20°	0.011	0.016	0.029		
30°	0.000	0.000	0.000	0.000	0.000

potential of the nuclear magnetic moment $\mathbf{A}^{\mathbf{m}_K}(\mathbf{r})$ multiplied by the current density $\boldsymbol{j}_e^{\mathbf{B}}(\mathbf{r})$. The nuclear magnetic shielding tensor $\boldsymbol{\sigma}$ can be calculated as the second derivative of the energy with respect to the strength of the external magnetic field and the nuclear magnetic moment in the limit of vanishing perturbations,

$$\sigma_{\alpha\beta}^{K} = -\frac{\partial^2}{\partial B_\beta \partial m_{K_\alpha}} \int \mathbf{A}^{\mathbf{m}_K}(\mathbf{r}) \cdot \boldsymbol{j}_e^{\mathbf{B}}(\mathbf{r}) d\mathbf{r} \Big|_{\substack{\mathbf{B}=\mathbf{0} \\ \mathbf{m}_K=\mathbf{0}}}. \tag{3}$$

The explicit expression for the magnetic shielding tensor is then given by

$$\sigma_{\alpha\beta}^{K} = -\sum_{\delta\gamma} \varepsilon_{\alpha\delta\gamma} \int \frac{r_\delta - R_{K\delta}}{|\boldsymbol{r} - \boldsymbol{R}_K|^3} \mathcal{J}_\gamma^{B_\beta}(\boldsymbol{r}) d\mathbf{r}, \tag{4}$$

where $\varepsilon_{\alpha\delta\gamma}$ is the Levi-Cività tensor for the three Cartesian directions [40]. The position of nucleus K is given by the vector $\boldsymbol{R}_K$ and the coordinates of the electrons are given by $\boldsymbol{r}$. Combining Eq. (4) with the analytic gradient expression for calculating nuclear magnetic shielding tensors and considering that the magnetic interaction obtained with the two expressions is the same at all points in space yields the GIMIC expression for calculating the current-density susceptibility. The tensor elements of the current-density susceptibility are given by

$$\begin{aligned}\mathcal{J}_\alpha^{B_\beta}(\boldsymbol{r}) = \sum_{\mu\nu} D_{\mu\nu} \Bigg(& \frac{\partial \omega_\mu^*(\boldsymbol{r})}{\partial B_\beta} \frac{\partial \tilde{h}(\boldsymbol{r})}{\partial m_{K,\alpha}} \omega_\nu(\boldsymbol{r}) + \omega_\mu^*(\boldsymbol{r}) \frac{\partial \tilde{h}(\boldsymbol{r})}{\partial m_{K,\alpha}} \frac{\partial \omega_\nu(\boldsymbol{r})}{\partial B_\beta} \\ & - \omega_\mu^*(\boldsymbol{r}) \omega_\nu(\boldsymbol{r}) \sum_\delta \varepsilon_{\alpha\beta\delta} \frac{\partial^2 \tilde{h}(\boldsymbol{r})}{\partial m_{K,\alpha} \partial B_\delta} \Bigg) \\ & + \sum_{\mu\nu} P_{\mu\nu}^{B_\beta} \omega_\mu^*(\boldsymbol{r}) \frac{\partial \tilde{h}(\boldsymbol{r})}{\partial m_{K,\alpha}} \omega_\nu(\boldsymbol{r}),\end{aligned} \tag{5}$$

where $D_{\mu\nu}$ and $P_{\mu\nu}^{B_\beta}$ are the density matrix and the magnetically perturbed density matrices with respect to the direction of the external magnetic field B_β, respectively, and $\omega_\mu^*(\boldsymbol{r})$ and $\omega_\nu(\boldsymbol{r})$ are gauge-including basis functions with the gauge origin at the center of the basis function [41]. The interaction of the nuclear magnetic moment with the external magnetic field is

$$\frac{\partial \tilde{h}(\boldsymbol{r})}{\partial \boldsymbol{m}_K} = (\boldsymbol{r} - \boldsymbol{R}_K) \times \boldsymbol{p}, \tag{6}$$

$$\frac{\partial^2 \tilde{h}(\boldsymbol{r})}{\partial \boldsymbol{m}_K \partial \boldsymbol{B}} = \tfrac{1}{2}[(\boldsymbol{r} - \boldsymbol{O}) \cdot (\boldsymbol{r} - \boldsymbol{R}_K)\mathbf{1} - (\boldsymbol{r} - \boldsymbol{O})(\boldsymbol{r} - \boldsymbol{R}_K)], \tag{7}$$

where $\boldsymbol{p}$ is the momentum operator, $\boldsymbol{m}_K$ is the nuclear magnetic moment of nucleus K, and $\boldsymbol{O}$ is the gauge origin. The singular denominator vanishes in the GIMIC expression, because the same singularity appears in all terms. The current-density susceptibility calculated using the GIMIC expression does not depend on the gauge origin. The current-density susceptibility depends only implicitly on the nuclear positions.

B. Analysis of the current density

The external magnetic field is directed along the C—C bond of the methyl group. This alignment ensures that the current density associated with electrons in the π orbitals of the phenyl group will largely vanish since the axis of the p orbitals is perpendicular to the magnetic field vector [35]. Therefore, in this study we mainly obtain current-density fluxes in the vicinity of the atomic nuclei and bond-current vortices that are due to electrons in σ orbitals.

The current density is calculated with GIMIC in discrete points in space. The streamline visual analysis is performed with the PARAVIEW program [42]. The streamline tool in PARAVIEW allows a sphere to be placed within the three-dimensional grid of the current-density vector field. Particles with a predefined density inside the sphere are then used for tracing the pathways of the vector field. A color scheme is applied where black corresponds to a very weak current density of 10^{-8} nA T^{-1} Å^{-2}, the middle tones go through red and yellow, and finally the largest magnitudes of the vectors of each grid point are drawn in white with a threshold of 0.09 nA T^{-1} Å^{-2}.

C. Strength of the current density

Calculations of the strength (I in nA T^{-1}) of the MIC in different parts of the molecule are performed by placing an integration plane through the molecule and integrating the current-density susceptibility vector $\boldsymbol{\mathcal{J}}^{B_\beta}(\boldsymbol{r})$ passing through its surface $\mathbf{S}$. The $\boldsymbol{\mathcal{J}}^{B_\beta}(\boldsymbol{r})$ is obtained from $\boldsymbol{\mathcal{J}}(\boldsymbol{r})$ by using a given direction of the external magnetic field B_β, which usually is parallel to the integration plane. The current-density strength is then given by

$$I = \iint_S \boldsymbol{\mathcal{J}}^{B_\beta}(\boldsymbol{r}) \cdot d\mathbf{S}. \tag{8}$$

The integration plane is split vertically into thin slices. Differential contributions to the MIC passing through the slices of the integration plane can be calculated as a function of the other coordinate of the plane yielding the current-density profile (in nA T^{-1} Å^{-1}). To ensure a high accuracy of the current-density profile, the width of the slices is 0.005 Å and the height is 4.2 Å for the two halves of the plane.

The current density is evaluated numerically using Gauss-Lobatto integration with 1233×9 grid points in each slice. The integration yields the strength of the current density in different parts of the molecule. The sign of the current density in each integration point corresponds to the direction of the current-density vector at the integration plane. The positive and negative contributions can be integrated separately. In one half of the integration plane, the positive contribution to the current density is the diatropic current density flowing in the classical direction with respect to the orientation of magnetic-field vector along the z axis, while the paratropic ring current is negative in the same half plane. In the other half of the integration plane, the returning current density has the opposite sign since the vortex loops back to the beginning. Integration of all contributions yields the net strength of the current density, which must vanish when the integration plane covers the whole molecule due to charge conservation.

Diatropic MICs flow in the classical direction and paratropic ones flow in the opposite direction. Tropicity is a global properties that can in principle be determined only by following the vector field around the whole vortex. However, for simple cases like the one studied here, the direction of the current density passing the whole integration plane can be used to determine the tropicity, whereas for complicated molecules it may be hard to distinguish between, for example, diatropic and returning paratropic current densities [43].

IV. MAGNETICALLY INDUCED CURRENT DENSITIES

A. Streamline representation

Streamline representations of the MIC of toluene are shown in Figs. 2 and 3. The external magnetic field is directed along the z axis, which almost coincides with the C—C bond to the methyl group. The C—C bond of the optimized structure deviates slightly from the z axis, which is due to steric interactions between the hydrogen atoms of the methyl group and the phenyl group. However, the tiny deviation of the C—C bond from the z axis does not significantly affect the results.

In the streamline plots, the chosen sphere radius is 0.53 Å. Figure 2 illustrates how the current density of the phenyl group extends at the C—C bond towards the *ipso* carbon atom forming a strong local current around the carbon atom. This current density corresponds to the large peak in the current-density profile seen in Fig. 4. In Fig. 3 the sphere was placed near the carbon atom of the phenyl group at the *ipso* position towards the CH_3 group. A strong current-density pathway circles the methyl group between the methyl carbon and its hydrogen atoms giving rise to shoulder next to the large carbon peak in Figs. 4 and 5. The strength of the current density flowing around the methyl group and the C—C bond to the methyl group is 10.41 nA T^{-1}, which is very close to the ring-current strength of benzene [44].

B. Integration of the strength of the current density

The current-density profile in Fig. 4 was obtained by placing an integration plane along the C—C bond to the methyl group cutting across the whole toluene molecule. The plane is perpendicular to the benzene ring as illustrated in Fig. 6. We analyzed separately the current-density profile for the two halves of the integration plane to avoid mixing of diatropic and returning paratropic current densities and vice versa.

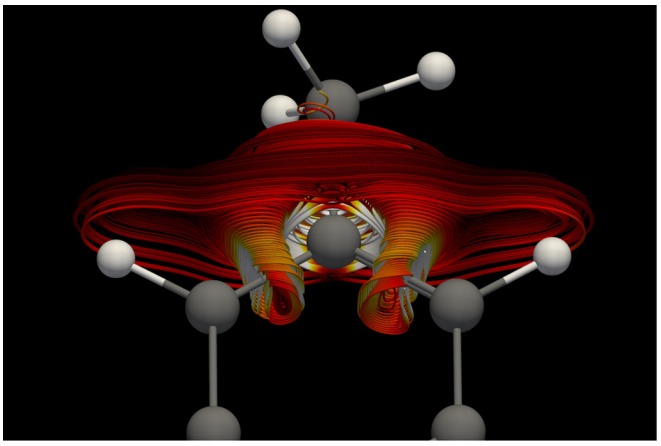

(a)

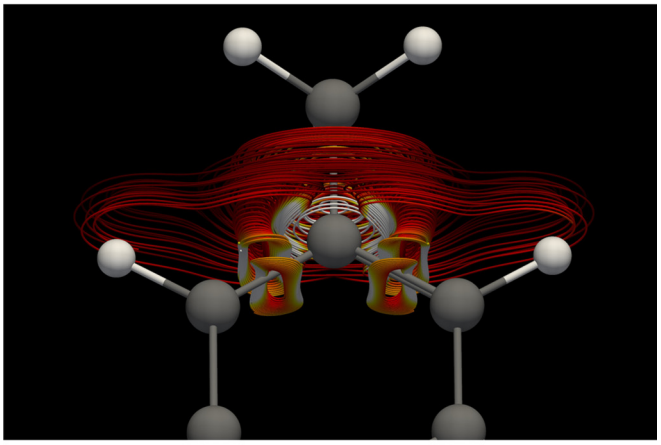

(b)

FIG. 2. (a) Streamline representation of the current density of the eclipsed ($\varphi = 0^\circ$) conformer of toluene and (b) streamline representation of the staggered ($\varphi = 30^\circ$) conformer. The current density is seen from the phenyl group.

The blue profile in Fig. 4 shows the diatropic current density passing the upper half of the integration plane in Fig. 6. The diatropic current density in the lower half has the opposite sign because it is the returning diatropic current density. The current-density profile in Fig. 4 deviates slightly from the one shown in Fig. 5, because the positions of the hydrogen atoms

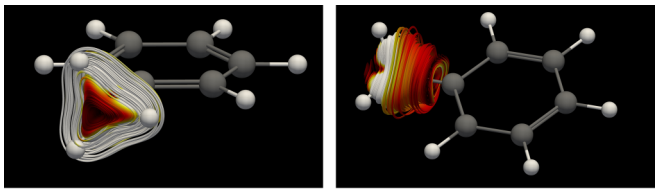

(a) (b)

FIG. 3. (a) Streamline representation of the current density at the methyl group of the eclipsed conformer ($\varphi = 0^\circ$) of toluene and (b) the other side (at the C—C bond) of the same streamline representation.

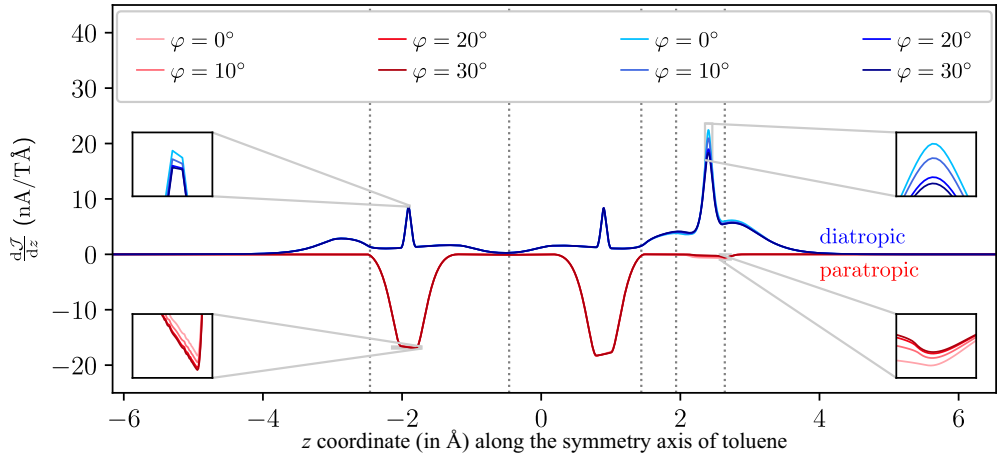

FIG. 4. Current-density profile of toluene (in nA T^{-1} $Å^{-1}$) along the z axis (in Å) showing where the current density passes through the upper half plane ($y > 0$) of the C_s symmetry plane intersecting the benzene ring and the methyl group. The vertical dotted lines divide the profile into atomic domains. The diatropic ring-current profiles calculated for different torsion angles φ are marked with blue nuances and the corresponding paratropic ones are reddish. The tiny differences in the current-density profile for different orientations of the hydrogen atoms of the methyl group are shown in the insets.

of the methyl group slightly differ and the methyl group is tilting slightly away from the symmetry axis. The profiles in Figs. 4 and 5 calculated for different torsional angles are also almost identical. Tiny differences are seen when enlarging parts of the profile, but the current-density flux through the plane is roughly the same regardless of the orientation of the hydrogen atoms of the methyl group. The color code in Figs. 4 and 5 represents the direction of the current density passing the integration plane. The vertical dashed bars indicate integration boundaries for the atomic domains studied.

The individual peaks in the current-density profile can be identified by comparing with the surface representation of the current-density flux in Fig. 7. The small diatropic peaks at the *ipso* and *para* carbon atoms originate from the 1s orbital of the carbon atoms, whereas the broad peaks at the *ipso* and *para* positions originate from the valence orbitals. The largest diatropic peak at the methyl group consists of contributions from the core orbital of the carbon atom and from the inner part of its valence orbitals. The shoulders to the left of the *para* carbon and to the right of the methyl carbon originate from the hydrogen atoms. The small paratropic contribution at the methyl carbon originates from a more diffuse part of the valence orbitals. The aromatic ring current is not present, because the external magnetic field is parallel to the aromatic ring.

The current-density vectors at the surface of the integration plane are shown in Fig. 7. The color scheme indicates the direction of the current-density field at each point on the plane. Blue and red denote positive and negative flux directions, respectively. Figure 7 shows the atomic current density

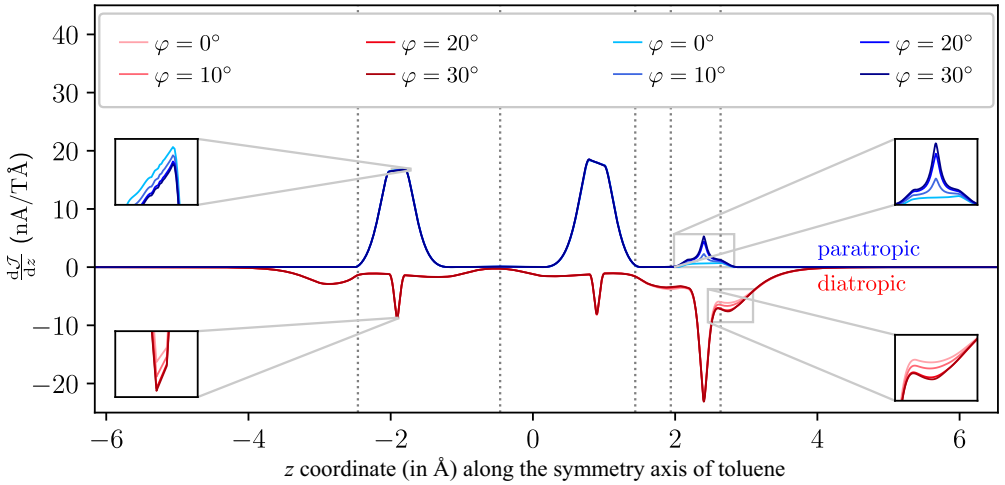

FIG. 5. Current-density profile of toluene (in nA T^{-1} $Å^{-1}$) along the z axis (in Å) showing where the current density passes through the lower half plane ($y < 0$) of the C_s symmetry plane intersecting the benzene ring and the methyl group. Since the diatropic ring current has the opposite sign on the other half of the plane intersecting the molecule, the profiles of the diatropic current density are marked in red and the corresponding paratropic ones are bluish. The tiny differences in the current-density profile for different orientations of the hydrogen atoms of the methyl group are shown in the insets.

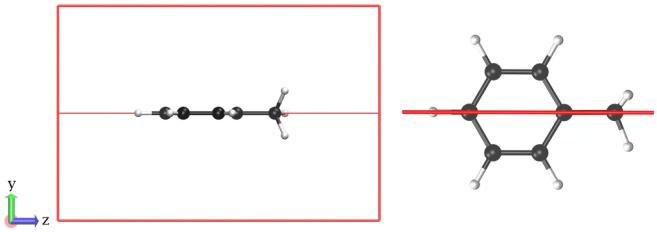

FIG. 6. Side and top views of the integration plane along the C—C bond for toluene. The two halves of the integration plane with $y < 0$ and $y > 0$ are investigated separately.

of the carbon atoms. The ipso and *para* C atoms have two vortices with circulation in the opposite direction; the current density in the core orbital is diatropic and that of the valence orbitals is paratropic. The carbon atom of the methyl group sustains a strongly diatropic current density that is surrounded by a weaker paratropic current density. The atomic current densities of sp^2 and sp^3 hybridized carbon atoms differ significantly. The current density is diatropic near the hydrogen atoms of the methyl group. One can also see that the whole molecule is surrounded by a weak diatropic current density. The current density passing through the plane in Fig. 7 is very similar for the eclipsed and the staggered structures.

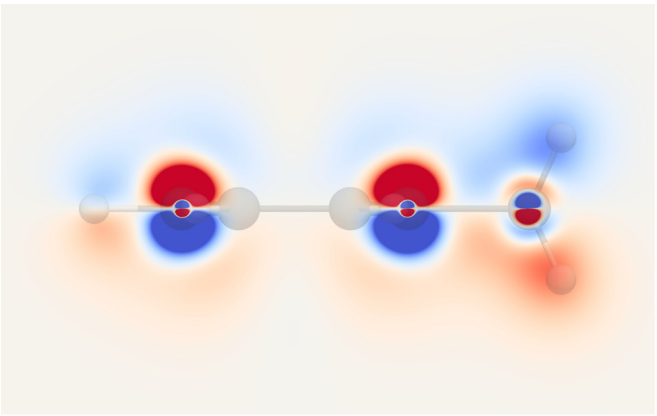

(a)

(b)

FIG. 7. (a) Surface representation of the current-density flux of the conformer with a torsion angle of $\varphi = 0^\circ$ (eclipsed). The current density is shown in the plane that is perpendicular to the toluene ring. The two hydrogen atoms of the methyl group point towards the viewer. (b) Corresponding picture of the staggered conformer ($\varphi = 30^\circ$). One hydrogen atom is on the integration plane pointing downward. The current-density vortices with red areas above the molecular plane are paratropic and diatropic current-density vortices are blue there, whereas the opposite color code holds below the plane.

The strength of the current density was analyzed quantitatively by splitting the integration domain into subdomains and separately integrating their current-density profile as shown in Fig. 4. The domain in the range $z \in [-6.0, -2.5]$ Å considers the current-density flux of the hydrogen atom in the *para* position. The domain of the *para* C atom is in the range of $z \in [-2.5, -0.5]$ Å. The domain of the *ipso* C atom is defined in the range of $z \in [-0.5, 1.4]$ Å. The domains of the C—C bond, the methyl carbon, and the hydrogen atoms of the methyl group are not well defined. We identified local minima in the current-density profile, which yielded estimated boundaries of the domains. We chose the domain of the C—C bond to be in the range of $z \in [1.4, 1.9]$ Å. The domain of the methyl carbon was chosen to be in the range of $z \in [1.9, 2.6]$ Å. The range of the domain of the methyl hydrogen atoms then becomes $z \in [2.6, 6.0]$ Å.

The integrated strengths of the current density in the individual domains calculated at the B3LYP def2-QZVP level are given in Table II. Since the conformers sustain almost the same current density in the domains, we discuss only the average current-density strengths. In the following, the absolute values of the differences between the current-density strengths of the eclipsed and staggered conformers are given in parentheses.

The total current strength passing through the integration plane is $-2.13(43)$ nA T^{-1} in the paratropic direction. Since calculations of the current density at the MP2 level yielded a positive current strength of 0.94(57) nA T^{-1}, we performed current-density calculations for the eclipsed structure at the CCSD(T) level, which yielded a total current strength of -1.93 nA T^{-1}. The total current strengths calculated at the B3LYP and CCSD(T) levels for the eclipsed conformer perfectly agree, even though it is known that common DFT functionals have difficulties in accurately treating the magnetic response of the core and semicore where the electron density is large [45]. Due to large canceling contributions from the methyl and phenyl groups, the total current strength is small, leading to opposite signs at the DFT and MP2 levels of theory. However, the individual current strengths of the methyl and phenyl groups are much larger, implying that qualitatively the same current strengths are obtained for them at the DFT and MP2 levels. In the DFT calculations, the largest paratropic contribution of $-14.90(6)$ nA T^{-1} originates from the *ipso* and *para* C atoms. The contribution from the *para* H atom is 2.36(3) nA T^{-1}. The three domains in the vicinity of the methyl group have a current strength of 10.41(51) nA T^{-1}, which is almost as strong as the ring current of benzene when the magnetic field is perpendicular to the ring.

The largest difference in the current-density distribution of the conformers of 0.72 nA T^{-1} appears at the methyl carbon, since the carbon atom of the methyl group does not lie exactly on the z axis, leading to a small current-density peak in Fig. 5 that does not appear in Fig. 4. The tiny positive contribution at the methyl group in Fig. 4 is actually not a paratropic

TABLE II. Strength (I in nA T^{-1}, where I is actually the integrated current susceptibility, since it is the first derivative of the current strength with respect to the strength of the external magnetic field in the limit of vanishing field strength) of the current density in the atomic domains of toluene calculated for different orientations of the methyl group. The current densities are calculated at the B3LYP/def2-QZVP level of theory. The difference in the strength of the current density of the eclipsed (0°) and staggered (30°) structures ($I_{\text{staggered}} - I_{\text{eclipsed}}$) are also reported. The results are for the electronic currents through the upper ($y > 0$) half plane (see Fig. 4).

Domain	0°	10°	20°	30°	Average	Difference
B3LYP[a]	−1.93	−2.03	−2.20	−2.36	−2.13	−0.43
para H atom, $z \in [-6.0; -2.5]$ Å	2.34	2.35	2.37	2.37	2.36	0.03
para C atom, $z \in [-2, 5; -0.5]$ Å	−7.02	−6.98	−6.95	−6.94	−6.97	0.08
ipso C atom, $z \in [-0.5; 1.4]$ Å	−7.91	−7.92	−7.93	−7.94	−7.93	−0.02
C—C bond, $z \in [1.4; 1.9]$ Å	1.52	1.48	1.45	1.44	1.47	−0.08
methyl C atom, $z \in [1.9; 2.6]$ Å	5.36	5.12	4.79	4.64	4.98	−0.72
methyl H atoms, $z \in [2.6; 6.0]$ Å	3.79	3.92	4.08	4.07	3.96	0.29
MP2[a,b]	1.20	1.01	0.90	0.63	0.94	0.57

[a]For the whole toluene molecule. The corresponding CCSD(T) value for the eclipsed (0°) structure is also −1.93 nA T^{-1}.
[b]Calculated at the MP2/def2-TZVPP level.

current density but a returning diatropic current density of the carbon atom of the methyl group, because the vortex center is not exactly on the integration plane. A diatropic current density of 3.96(29) nA T^{-1} is sustained in the domain of the hydrogen atoms of the methyl group, which is seen in Fig. 3. The energetically lowest conformer with a torsion angle of 30° sustains a 0.43 nA T^{-1} weaker net current density than the eclipsed conformer with a torsion angle of 0°, since the sum of the current density at the methyl group and the one at the C—C bond is 0.52 nA T^{-1} weaker for the staggered structure.

V. DISCUSSION AND CONCLUSIONS

The magnetically induced electronic ring current sustained by toluene when the magnetic field is directed along the C—C bond between the phenyl ring and the methyl group can be divided into a diatropic ring current of 10.41(51) nA T^{-1} around the methyl group and a slightly stronger paratropic ring current of −12.54(9) nA T^{-1} around the phenyl group. Since the magnetic field is parallel to the phenyl ring, its π orbitals do not contribute significantly to the ring current around the phenyl group. The ring-current strength is almost independent of the orientation of the hydrogen atoms of the methyl group. The magnetically induced nuclear ring current sustained by toluene of 19.9 pA T^{-1} [1] is two orders of magnitude smaller than the electronic ring current of −2.13(43) nA T^{-1} obtained in the DFT calculations. The MP2 and CCSD(T) calculations for the eclipsed conformer yielded current strengths of 1.20 nA T^{-1} and −1.93 nA T^{-1}, respectively. The electronic ring current is weakly paratropic at the DFT and CCSD(T) levels, whereas it is weakly diatropic at the MP2 level. The diatropic and paratropic contributions to the current strength obtained at the three computational levels qualitatively agree. However, due to cancellation of large contributions from the methyl and the phenyl groups, the opposite sign is obtained at the MP2 level compared to the DFT and CCSD(T) calculations.

To detect nuclear ring currents, either the phenyl group or the methyl group must be fixed in the experimental setup. It is probably easier to block the rotation of the phenyl group than to prevent the rotation of the methyl group when the C—C bond between the phenyl and methyl groups is aligned with the direction of the magnetic field. In such an experiment only the ring currents of the methyl group are relevant. Electronic and nuclear current densities might be detected in neutron scattering experiments [46–48]. The nuclear contribution is 3.7 pA T^{-1} [1], which is more than three orders of magnitude smaller than the electronic contribution of 10.41 nA T^{-1}. Assuming that the methyl group is fixed and the phenyl group can rotate, the nuclear contribution is 16.3 pA T^{-1}, compared to the electronic contribution of −12.54 nA T^{-1}.

The bare nucleus approximation was assumed in the calculation of nuclear ring currents. The nuclei are surrounded by an electron density that rotates with the nuclei. Population analysis shows that the effective charge of the methyl hydrogen atoms is $0.21e$ instead of $1e$ in the bare nucleus approximation. The effective nuclear ring current of the methyl group is then about 1 pA T^{-1} when considering the effective charge of the hydrogen atoms of the methyl group.

The charge of the *ortho* and *meta* carbon atoms is $-0.21e$ and $-0.20e$, respectively. The effective charge of the *ortho* and *meta* hydrogen atoms are $0.20e$ and $0.21e$, respectively. Thus, the nuclear ring current of the phenyl ring is practically canceled by the ring current due to the electron density circulating with nuclei. Detection of the nuclear ring current of the phenyl group is therefore difficult, whereas it might be possible to observe the circulating effective charge of the hydrogens of the methyl group.

Magnetic shielding effects also affect the nuclear current density, because the strength of the magnetic field experienced by the nuclei in the molecule differs from the applied one. However, for hydrocarbons such as toluene, the magnetic shielding of the hydrogen nuclei is of the order of 25–30 ppm and for the carbon nuclei it is two to six times larger. Thus, very strong magnetic fields are required before the effect of the magnetic shielding is as important as the electric shielding effect [49–54].

ACKNOWLEDGMENTS

This work was supported by the Academy of Finland through Projects No. 314821 and No. 340583, the

Swedish Cultural Foundation in Finland, the National Key Research and Development Program of China (Grant No. 2017YFA0304203), Natural Science Basic Research Program of Shaanxi (Grant No. 2022JQ-062), the Program for Changjiang Scholars and Innovative Research Team (Grant No. IR_17R70), the National Natural Science Foundation of China (Grant No. 11904215), the 111 project (Grant No. D18001), the Fund for Shanxi 1331 Project, and the Hundred Talent Program of Shanxi Province. M.D. thanks the Finnish Cultural Foundation for a research grant.

[1] D. Jia, M. Dimitrova, Y. Man, D. Sundholm, and Y. Yang, preceding paper, Phys. Rev. A **106**, 042801 (2022).
[2] V. V. Ilyushin, Z. Kisiel, L. Pszczókowski, H. Mäder, and J. T. Hougen, J. Mol. Spectrosc. **259**, 26 (2010).
[3] J. R. Gascooke, E. A. Virgo, and W. D. Lawrance, J. Chem. Phys. **142**, 024315 (2015).
[4] T. Grohmann, D. Haase, D. Jia, J. Manz, and Y. Yang, J. Chem. Phys. **149**, 184302 (2018).
[5] J. Jusélius, D. Sundholm, and J. Gauss, J. Chem. Phys. **121**, 3952 (2004).
[6] S. Taubert, D. Sundholm, and J. Jusélius, J. Chem. Phys. **134**, 054123 (2011).
[7] H. Fliegl, S. Taubert, O. Lehtonen, and D. Sundholm, Phys. Chem. Chem. Phys. **13**, 20500 (2011).
[8] D. Sundholm, H. Fliegl, and R. J. F. Berger, WIREs Comput. Mol. Sci. **6**, 639 (2016).
[9] D. Sundholm, M. Dimitrova, and R. J. F. Berger, Chem. Commun. **57**, 12362 (2021).
[10] H. Fliegl, R. Valiev, F. Pichierri, and D. Sundholm, in *Chemical Modelling*, edited by M. Springborg and J.-O. Joswig (Royal Society of Chemistry, Cambridge, 2018), Vol. 14, pp. 1–42.
[11] K. Reiter, F. Weigend, L. N. Wirz, M. Dimitrova, and D. Sundholm, J. Phys. Chem. C **123**, 15354 (2019).
[12] M. Dimitrova and D. Sundholm, in *Aromaticity: Modern Computational Methods and Applications*, edited by I. Fernández López (Elsevier, Amsterdam, 2021), Chap. 5, pp. 155–194.
[13] D. Sundholm and H. Fliegl, in *Handbook of Porphyrin Science*, edited by K. M. Kadish, K. M. Smith, and R. Guilard (World Scientific, Singapore, 2022), Vol. 46, p. 218.
[14] A. D. Becke, J. Chem. Phys. **98**, 5648 (1993).
[15] C. Lee, W. Yang, and R. G. Parr, Phys. Rev. B **37**, 785 (1988).
[16] F. Weigend and R. Ahlrichs, Phys. Chem. Chem. Phys. **7**, 3297 (2005).
[17] S. Grimme, J. Antony, S. Ehrlich, and H. Krieg, J. Chem. Phys. **132**, 154104 (2010).
[18] R. Ahlrichs, M. Bär, M. Häser, H. Horn, and C. Kölmel, Chem. Phys. Lett. **162**, 165 (1989); available at http://www.turbomole.com.
[19] F. Furche, R. Ahlrichs, C. Hättig, W. Klopper, M. Sierka, and F. Weigend, WIREs Comput. Mol. Sci. **4**, 91 (2014).
[20] S. G. Balasubramani, G. P. Chen, S. Coriani, M. Diedenhofen, M. S. Frank, Y. J. Franzke, F. Furche, R. Grotjahn, M. E. Harding, C. Hättig *et al.*, J. Chem. Phys. **152**, 184107 (2020).
[21] O. Treutler and R. Ahlrichs, J. Chem. Phys. **102**, 346 (1995).
[22] F. Weigend and M. Häser, Theor. Chem. Acc. **97**, 331 (1997).
[23] S. Grimme, L. Görigk, and R. F. Fink, WIREs Comput. Mol. Sci. **2**, 886 (2012).
[24] M. Häser, R. Ahlrichs, H. P. Baron, P. Weis, and H. Horn, Theor. Chim. Acta **83**, 455 (1992).
[25] M. Kollwitz, M. Häser, and J. Gauss, J. Chem. Phys. **108**, 8295 (1998).
[26] K. Reiter, F. Mack, and F. Weigend, J. Chem. Theory Comput. **14**, 191 (2018).
[27] J. Gauss and J. F. Stanton, J. Chem. Phys. **104**, 2574 (1996).
[28] F. Jensen, J. Chem. Theory Comput. **10**, 1074 (2014).
[29] J. F. Stanton, J. Gauss, L. Cheng, M. E. Harding, D. A. Matthews, P. G. Szalay, *et al.*, CFOUR, a quantum chemical program package; the integral packages by J. Almlöf and P. R. Taylor, MOLECULE; P. R. Taylor, PROPS; T. Helgaker, H. J. A. Jensen, P. Jørgensen, and J. Olsen, ABACUS; A. V. Mitin and C. van Wüllen, ECP routines. The current version is available at http://www.cfour.de.
[30] M. E. Harding, T. Metzroth, J. Gauss, and A. A. Auer, J. Chem. Theory Comput. **4**, 64 (2008).
[31] D. A. Matthews, L. Cheng, M. E. Harding, F. Lipparini, S. Stopkowicz, T.-C. Jagau, P. G. Szalay, J. Gauss, and J. F. Stanton, J. Chem. Phys. **152**, 214108 (2020).
[32] J. Jusélius, D. Sundholm *et al.*, GIMIC, version 2.0, a current density program, available at https://github.com/qmcurrents/gimic.
[33] R. M. Stevens, R. M. Pitzer, and W. N. Lipscomb, J. Chem. Phys. **38**, 550 (1963).
[34] C. J. Jameson and A. D. Buckingham, J. Phys. Chem. **83**, 3366 (1979).
[35] P. Lazzeretti, Prog. Nucl. Magn. Reson. Spectrosc. **36**, 1 (2000).
[36] P. Lazzeretti, J. Chem. Phys. **148**, 134109 (2018).
[37] K. Wolinski, J. F. Hinton, and P. Pulay, J. Am. Chem. Soc. **112**, 8251 (1990).
[38] T. Helgaker, M. Jaszuński, and K. Ruud, Chem. Rev. **99**, 293 (1999).
[39] J. Gauss and J. F. Stanton, Adv. Chem. Phys. **123**, 355 (2002).
[40] A. A. Evett, Am. J. Phys. **34**, 503 (1966).
[41] R. Ditchfield, Mol. Phys. **27**, 789 (1974).
[42] J. Ahrens, B. Geveci, and C. Law, *Paraview: An End-User Tool for Large Data Visualization* (Elsevier, Amsterdam, 2005), available at https://www.paraview.org.
[43] D. Sundholm, R. J. F. Berger, and H. Fliegl, Phys. Chem. Chem. Phys. **18**, 15934 (2016).
[44] H. Fliegl, D. Sundholm, S. Taubert, J. Jusélius, and W. Klopper, J. Phys. Chem. A **113**, 8668 (2009).
[45] S. Reimann, U. Ekström, S. Stopkowicz, A. M. Teale, A. Borgoo, and T. Helgaker, Phys. Chem. Chem. Phys. **17**, 18834 (2015).
[46] C. Wilkinson, D. A. Keen, P. J. Brown, and J. B. Forsyth, J. Phys.: Condens. Matter **1**, 3833 (1989).
[47] C. Stassis, Phys. Rev. Lett. **24**, 1415 (1970).
[48] S. Nandi, Y. Xiao, Y. Su, L. C. Chapon, T. Chatterji, W. T. Jin, S. Price, T. Wolf, P. J. Brown, and T. Brückel, Phys. Rev. B **88**, 184413 (2013).
[49] D. Ceresoli, R. Marchetti, and E. Tosatti, Phys. Rev. B **75**, 161101(R) (2007).
[50] L. Yin and C. Alden Mead, J. Chem. Phys. **100**, 8125 (1994).
[51] T. Detmer, P. Schmelcher, and L. S. Cederbaum, J. Phys. B **28**, 2903 (1995).

[52] T. Detmer, P. Schmelcher, F. K. Diakonos, and L. S. Cederbaum, in *Atoms and Molecules in Strong External Fields*, edited by P. Schmelcher and W. Schweizer (Springer US, Boston, 2002), pp. 275–282.

[53] T. Culpitt, L. D. M. Peters, E. I. Tellgren, and T. Helgaker, J. Chem. Phys. **155**, 024104 (2021).

[54] L. D. M. Peters, T. Culpitt, L. Monzel, E. I. Tellgren, and T. Helgaker, J. Chem. Phys. **155**, 024105 (2021).

Correction: The previously published Figures 4 and 5 contained a sign error and have been replaced.